A Time Efficient Optical Model for GATE Simulation of a LYSO Scintillation Matrix Used in PET Applications

Daniel A. B. Bonifacio, Nicola Belcari, Sascha Moehrs, Mauricio Moralles, Valeria Rosso, Sara Vecchio, and Alberto Del Guerra, *Senior Member, IEEE*

***Abstract*—A time efficient optical model is proposed for GATE simulation of a LYSO scintillation matrix coupled to a photomultiplier. The purpose is to avoid the excessively long computation time when activating the optical processes in GATE. The usefulness of the model is demonstrated by comparing the simulated and experimental energy spectra obtained with the dual planar head equipment for dosimetry with a positron emission tomograph (DoPET). The procedure to apply the model is divided in two steps. Firstly, a simplified simulation of a single crystal element of DoPET is used to fit an analytic function that models the optical attenuation inside the crystal. In a second step, the model is employed to calculate the influence of this attenuation in the energy registered by the tomograph. The use of the proposed optical model is around three orders of magnitude faster than a GATE simulation with optical processes enabled. A good agreement was found between the experimental and simulated data using the optical model. The results indicate that optical interactions inside the crystal elements play an important role on the energy resolution and induce a considerable degradation of the spectra information acquired by DoPET. Finally, the same approach employed by the proposed optical model could be useful to simulate a scintillation matrix coupled to a photomultiplier using single or dual readout scheme.**

***Index Terms*—Monte Carlo methods, optical signal detection, positron emission tomography, scintillation detectors.**

I. Introduction

MONTE CARLO simulation is a very useful tool for the assessment of the performance of medical imaging devices in emission tomography, for the optimization of acquisition protocols, and for the development of image reconstruction algorithms and correction techniques [1]. The GATE (Geant4 Application for Emission Tomography) [2] simulation code, which is based on Geant4 toolkit [3], is widely used for those tasks [4]–[6]. GATE features description of time-dependent processes, acquisition and signal processing stage for a complete system simulation. However, activating optical processes in GATE makes the simulation about three orders of magnitude slower [7], becoming highly time consuming. The aim of this work is to propose a time efficient optical model for GATE simulation of a LYSO scintillation matrix coupled to a photomultiplier (PMT), as used in several PET applications [8]–[10]. The optical model describes the light attenuation inside the crystal, which depends on the DOI (Depth Of Interaction), and its posterior collection by the PMT.

The usefulness of the model is demonstrated by comparing the simulated and experimental energy spectra obtained with the dual planar head equipment for dosimetry with a positron emission tomograph (DoPET) [11]. DoPET features a channel-to-energy calibration procedure that uses as energy reference the 511 keV peak from a $^{22}\mathrm{Na}$ source and also considers that the number of collected optical photons by the PMT is proportional to the deposited gamma energy. The light attenuation inside the crystal, which depends on the position of the interaction of the gamma rays and occurs during the light transport before being collected by the PMT, deteriorates asymmetrically the energy resolution of the detector and cannot be corrected for absolute calibration purposes because of the single side PMT readout scheme.

An evident example of the blurring of the energy resolution of DoPET is the energy spectrum, acquired in single mode, of the $^{176}\mathrm{Lu}$ intrinsic radioactivity present in LYSO crystal. The abundance of $^{176}\mathrm{Lu}$ in the lutetium is about 2.6% and it has a half-life of 3.78×10^{10} years. Consequently, the background count rate registered over an acquisition in single mode is approximately 240 $\mathrm{cps/cm^3}$ [12]. According to the $^{176}\mathrm{Lu}$ decay scheme (Fig. 1), the expected maximum energy value in the measured spectrum is around 1.2 MeV. However, DoPET calibration and position dependence of the light attenuation inside the crystal make DoPET register this maximum energy value in a range between 1.2 and 1.8 MeV (Fig. 2).

Thus, the transport of optical photons was included in our simulation with the purpose to reproduce the measured results. The proposed optical model was used in order to avoid the excessively long computation time from GATE optical processes.

II. Material and Methods

A. DoPET Design

DoPET (Fig. 3) consists of two planar heads, each one composed of one array of 21 $\times$ 21 optically isolated LYSO

Manuscript received November 09, 2009; revised March 22, 2010 and July 09, 2010; accepted July 22, 2010. Date of publication September 13, 2010; date of current version October 15, 2010. This work was supported by the Brazilian agencies CNPq and CAPES.

D. A. B. Bonifacio is with the Institute of Physics-University of Sao Paulo, Nuclear and Energy Research Institute-Ipen/CNEN/SP-Brazil, 05508-000 Sao Paulo, Brazil and also with the Department of Physics "E. Fermi", University of Pisa, 57126 Pisa, Italy (e-mail: daniel@if.usp.br).

N. Belcari, V. Rosso, S. Vecchio, and A. Del Guerra are with the Department of Physics "E. Fermi", University of Pisa, 57126 Pisa, Italy and also with INFN-Pisa, 56127 Pisa, Italy.

S. Moehrs is with the Department of Physics "E. Fermi", University of Pisa, 57126 Pisa, Italy.

M. Moralles is with the Nuclear and Energy Research Institute-Ipen/CNEN/SP-Brazil, 05508-000 Sao Paulo, Brazil.

Color versions of one or more of the figures in this paper are available online at http://ieeexplore.ieee.org.

Digital Object Identifier 10.1109/TNS.2010.2062536

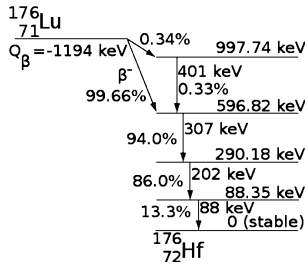

Fig. 1. ^{176}Lu decay scheme to ^{176}Hf [13]. In 99.66% of the cases, ^{176}Lu decays into ^{176}Hf by beta-emission with a maximum energy of 597.18 keV, followed by a cascade of gamma photons with energies of 307, 202 and 88 keV.

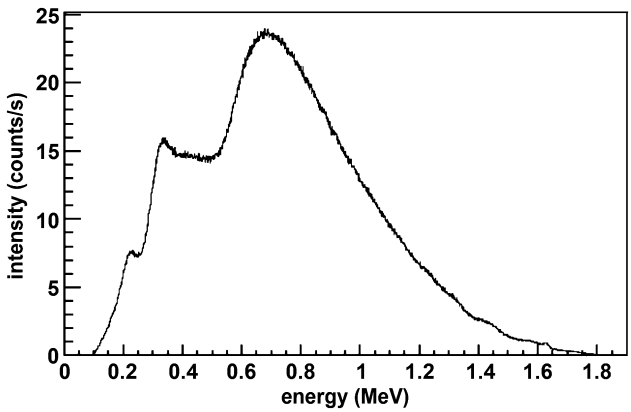

Fig. 2. Spectrum of the ^{176}Lu intrinsic radioactivity measured by the DoPET detector matrix. The energy scale was calibrated linearly using the 511 keV photopeak.

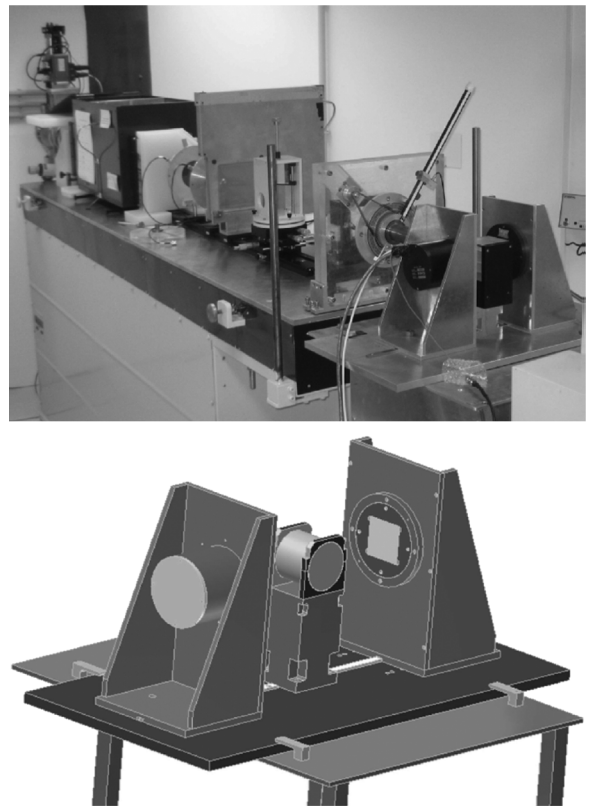

Fig. 3. Photo of the DoPET apparatus at the end of the proton beam line and a schematic view of DoPET. The two planar detector heads and the plastic cylindrical phantom are held by an alluminum-alloy support. The equipment is positioned on a plane which is aligned with respect to the beam direction. Protons impinge on one base of the cylindrical phantom [11].

($Lu_{2(1-x)}Y_{2x}SiO_5$, $x \approx 0.1$) crystal elements from Hilger Crystals Ltd (UK), a Hamamatsu H8500C flat panel photomultiplier (PMT) and associated electronics for signal amplification and digitization.

Each LYSO element is $2\ \mathrm{mm} \times 2\ \mathrm{mm} \times 18\ \mathrm{mm}$ with both end faces polished. The remaining four sides did not receive any surface treatment, left unpolished as they were mechanically cut. Each array is constructed using white epoxy as the reflector material with 0.15 mm of separator thickness. One of the faces is covered by three layers of a 0.08 mm thick PTFE reflector tape (Saint Gobain BC-642) and the other face is optically coupled to a photomultiplier (PMT) using a mounting media (Cargille Meltmount 1.582). The H8500C PMT has an active area of $49\ \mathrm{mm} \times 49\ \mathrm{mm}$, 8×8 channels multi-anode, bialkali photo-cathode and borosilicate window. The number of acquired signals is reduced from 64 to 4 signals per head by means of a multiplexed read-out [14].

B. Proposed Optical Model Overview

The procedure to apply the model is divided in two steps. Firstly, a simplified simulation of a single crystal element of DoPET is used to obtain the optical attenuation as a function of the distance between the point where the light emission occurs and the PMT. The results of this simulation is used to fit an analytic function that models the light attenuation. In a second step, the model is employed to calculate the influence of this attenuation in the energy registered by the tomograph. All the simulations were performed using GATE version 4.0.0, which is based on Geant4 version 9.1.p02.

The following analytical function was employed to fit the number of optical photons "N_{ph}" collected by the PMT after the total energy deposition of a 511 keV annihilation gama ray at a distance "z" from the PMT window:

$$N_{ph}(z) = A\exp(-z/\lambda_1) + B\exp(z/\lambda_2) \qquad (1)$$

where there are four adjusted parameters represented by "A", "B", "λ_1" and "λ_2". This function models the combination of all physical processes involved in the light attenuation through the scintillator slab and its posterior collection by the PMT.

The input data are the mean values of the number of detected optical photons for a set of distances z. This set varies from 0.5 mm to 17.5 mm by 1 mm steps. They are obtained from a simplified simulation with the optical processes activated, which consists of 511 keV gamma rays interacting and depositing all their energy at the center of a single crystal element along its longitudinal axis. Simulations of 511 keV gamma rays interacting out of the center of the crystal presented results that are statistically equivalent to those at the center of the crystal. The simulation is illustrated in Fig. 4, which also shows the relevant materials and their optical couplings. The single crystal is located at the center of the PMT. Since the PMT area is larger than the matrix area, the difference of light collection between a crystal located

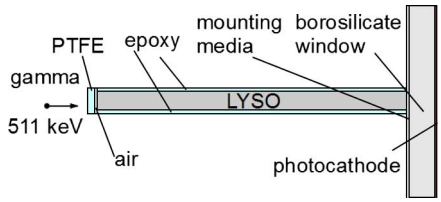

Fig. 4. Simplified scheme of the simulated optical layers, volumes and materials used in GATE.

at the edge of the PMT and at the center of the PMT was considered negligible.

If the crystal is linear in respect with the light yield, it is possible to use (1) to obtain the number of optical photons collected by the PMT for any value of deposited energy inside the crystal according to the DOI.

Thus, the complete simulation for the DoPET detector was performed using all the relevant interactions, except the time consuming optical processes, and (1) was applied on (2) to determine the registered energy $(\mathrm{E_{reg}})$ by the detector:

$$\mathrm{E_{reg}} = \mathrm{E_{dep}}\,(\mathrm{N_{ph}(z)}/\mathrm{N_{ph511}}) \tag{2}$$

where the energy value $\mathrm{E_{dep}}$—originated from the "Hits" data output—is the deposited energy inside the crystal for each event and $\mathrm{N_{ph511}}$ is the number of optical photons corresponding to the 511 keV peak used in the energy calibration.

The probability of encountering a 511 keV gamma at a certain depth z into the crystal is given by [15]:

$$\mathrm{P(z)} = \exp\left(-(\mathrm{L}-\mathrm{z})\mu_{511}\right) \tag{3}$$

where μ_{511} is the attenuation coefficient of LYSO for 511 keV. From (3), the energy deposition of the 511 keV photons occurs with the highest probability in the frontal region of each crystal element, which is furthest away from the PMT. Thus, for calibration purposes, it was assumed that $\mathrm{Nph_{511}}$ corresponds to the position at the front of the crystal.

1) Simplified Simulation Aspects: Optical Processes Active: To find the fitting parameters of (1), a simulation with the following simplifications was used. With respect to the physical processes involving gamma interactions, only the photoelectric effect from the Standard physical model was activated in GATE, while Compton and Rayleigh scattering remained inactive. The electron cut is given in range and it was set to 30 cm to avoid secondary electron production. This value means that the secondary electron would be generated only when its range is greater than 30 cm. Thus, for each interaction occurring inside the crystal all the gamma energy is deposited at once in a specific region, where the optical photons are generated.

While scintillation is responsible for the optical photon production, the physical processes concerning optical photon interactions are optical absorption, optical Rayleigh scattering, as well as refraction and reflection on the surfaces. These processes require the definition of some specific material properties.

LYSO properties comprise light yield (32 photons/keV), time decay constant (41 ns) and emission peak wavelength (420 nm),

TABLE I
INDEX OF REFRACTION OF LYSO CRYSTAL [17]

wavelength (nm)	index of refraction
405	1.833
420	1.827
436	1.822
461	1.818
486	1.813
516	1.810
546	1.806

TABLE II
PROPERTIES FOR LYSO-PTFE AND LYSO-EPOXY SURFACES

Name	LYSO-PTFE	LYSO-Epoxy
model	UNIFIED	UNIFIED
type	dielectric_dielectric	dielectric_dielectric
finish	groundbackpainted	groundbackpainted
σ_α	0.1 degrees	4.0 degrees
$\mathrm{N_{RC}}$	1.0 (air)	1.53 (epoxy)
$\mathrm{C_{SL}}$	1	1
$\mathrm{C_{SS}}$	0	0
$\mathrm{C_{BS}}$	0	0
reflectivity	0.98	0.94
efficiency	0	0

as provided by the manufacturer. Absorption length $(\lambda_{\mathrm{ab}} = 50\ \mathrm{cm})$ and Rayleigh scattering length $(\lambda_{\mathrm{sc}} = 260\ \mathrm{cm})$ were constrained to a total attenuation length $(\lambda_{\mathrm{ef}} = 42\ \mathrm{cm})$ from [16] and the relation:

$$1/\lambda_{\mathrm{ef}} = 1/\lambda_{\mathrm{ab}} + 1/\lambda_{\mathrm{sc}} \tag{4}$$

where $\lambda_{\mathrm{ef}} \approx 0.8\lambda_{\mathrm{ab}}$ for LYSO [16].

The index of refraction was set as a function of the optical photon wavelength [17], as can be seen in Table I.

White epoxy, PTFE tape, mounting media and borosilicate window were assumed to have an index of refraction of 1.53, 1.34, 1.582 and 1.51, respectively.

It is known that self-absorption is usually not a significant loss mechanism [15]. However, refraction and reflection on the surfaces play an important role in the present simulations. Geant4 provides two implementations of optical boundary process: GLISUR and UNIFIED models [18], [19], but only the UNIFIED model can be used under the GATE framework. Thus, the "GateSurface" class was changed to permit also the use of the GLISUR optical model, which was chosen to simulate a dielectric_metal surface using the complex index of refraction of a metal, like the bialkali photo-cathode of a PMT.

Table II shows the properties adopted for the surface between LYSO crystal and epoxy layer and the surface between LYSO crystal and PTFE tape.

In the UNIFIED model, a ground surface is formed by microfacets whereas each one has a normal vector which deviates from the mean normal by an angle α (Fig. 5). Thus, the roughness of this surface is defined by σ_α, which is the standard deviation of the Gaussian distribution of angles α.

$\mathrm{N_{RC}}$ is the index of refraction of the reflective coat. The probability of occurring the various reflection mechanisms pro-

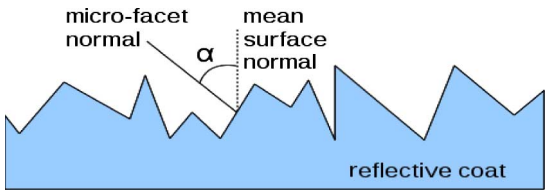

Fig. 5. Micro-facets in a ground surface, according to the UNIFIED model.

TABLE III
COMPLEX INDEX OF REFRACTION OF PMT'S PHOTO-CATHODE [21]

wavelength (nm)	complex index of refraction real (n)	imaginary (k)
380	1.92	1.69
395	2.18	1.69
410	2.38	1.71
425	2.61	1.53
440	2.70	1.50
470	3.00	1.34
530	3.26	0.86
590	3.01	0.42
680	2.96	0.33

TABLE IV
QUANTUM EFFICIENCY OF PMT H8500 [22]

wavelength (nm)	quantum efficiency
305	0.24
350	0.27
400	0.26
420	0.24
450	0.20
500	0.15
600	0.01
675	0.001

vided by the UNIFIED model are defined by four constants. C_{SL} stands for specular lobe constant and represents the probability of specular reflection about the normal of a micro facet. C_{SS} means specular spike constant and represents the specular reflection probability about the average surface normal. C_{BS} is the back scatter constant which sets the probability of backward reflection and has more influence on very rough surfaces. The diffuse lobe constant (C_{DL}) represents the probability of internal Lambertian reflection. The sum of the four constants must be one and the diffuse lobe constant is defined implicitly through the relation $C_{DL} = 1 - (C_{SL} + C_{SS} + C_{BS})$.

As it was impossible to obtain σ_α experimentally, because we received the crystal arrays already mounted in the epoxy resin, we assumed that a smooth surface has $\sigma_\alpha = 0.1$ [20]. For a saw-cut surface we used the value that best matches our results $(\sigma_\alpha = 4.0)$.

The surface type dielectric_metal and finish polished from the GLISUR model were employed in the surface between PMT window and its photo-cathode, which has a complex index of refraction [21] and quantum efficiency [22] with values described in Tables III and IV, respectively.

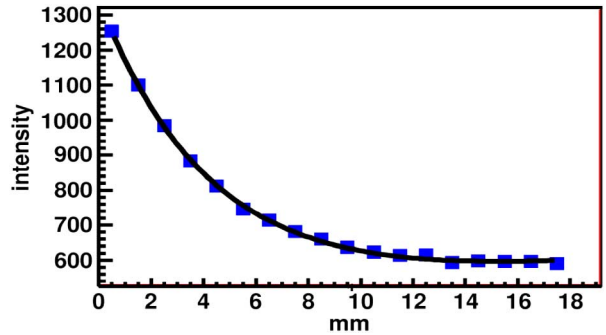

Fig. 6. Mean number of optical photons detected by the PMT according to the position of the deposited gamma energy inside a single crystal.

Moreover, all other surfaces were assumed to have properties commonly used in a dielectric/dielectric smooth surface: UNIFIED model, ground finish, $\sigma_\alpha = 0.1$ degrees and specular lobe constant 1.

2) Complete Simulation Aspects: Applying the Optical Model: The selected physical processes for the complete DoPET simulation were photoelectric effect and Compton and Rayleigh scattering from the Low Energy physical model. The optical model presented in the previous section was employed instead of activating the optical processes simulation. Currently, the readout module of GATE determine the position of the gamma interaction in the crystal matrix as being the position of the crystal where the highest energy was deposited. Thus, the "GateReadout" class was modified to calculate the position of the gamma interaction based on a PMT using the Anger logic configuration. The energy resolution at 511 keV was set to 15.4% (FWHM) as measured experimentally and a coincidence window of 10 ns was used. Finally, the distance between the two detector heads was kept at 14 cm.

We performed simulations with and without the use of the optical model to compare them with the experimental results from DoPET. The comparisons were done for acquisitions in single and coincidence modes. The particle-emitting isotopes were simulated using the General Particle Source (GPS) module [23] provided by Geant4. One simulation consisted of an acquisition of the ^{176}Lu intrinsic radioactivity present in the LYSO crystal and was performed by filling the crystal volume with an uniform distribution of ^{176}Lu. The other simulation took into consideration the same LYSO background activity together with a ^{22}Na point-like source defined as a sphere with 0.5 mm of radius and placed at the center of the field of view of DoPET.

III. RESULTS

Fig. 6 shows the relation between the mean number of optical photons detected by the PMT and the position of the deposited gamma energy inside a single crystal, calculated with the methodology described in Section II-B. The fitted function (1) has the following parameters: $A = 851$ photons, $\lambda_1 = 4.31$ mm, $B = 491$ photons, $\lambda_2 = 100$ mm. The light collection at the PMT decreases with the distance of the interaction point to the PMT. At the extremity of the crystal its value falls to less than half of the intensity calculated at the nearest point from the PMT.

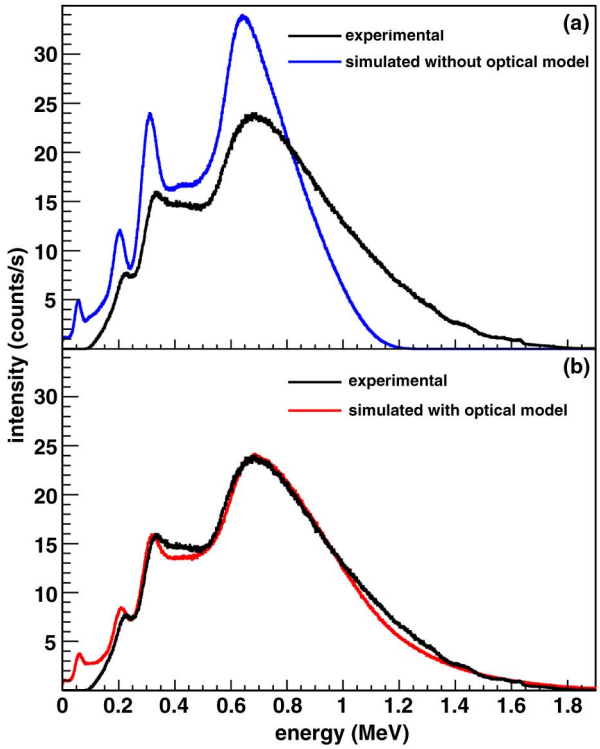

Fig. 7. Comparison of the simulated DoPET spectra without (a) and with (b) the use of the optical model, with the measured spectrum of the LYSO crystal intrinsic radioactivity (^{176}Lu) acquired in single mode.

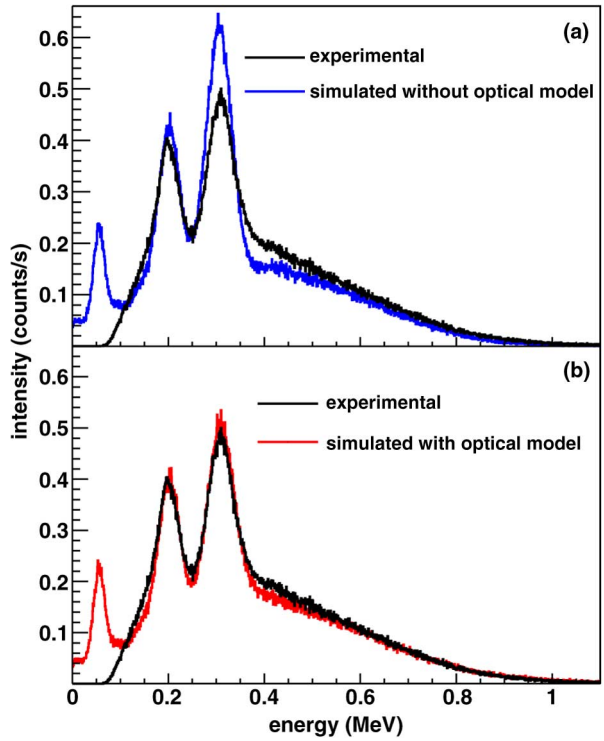

Fig. 8. Comparison of the simulated DoPET spectra without (a) and with (b) the use of the optical model, with the measured spectrum of the LYSO crystal intrinsic radioactivity (^{176}Lu) acquired in coincidence mode.

The number of optical photons at the extremity of the crystal element (18 mm) is the one associated with the 511 keV peak ($N_{ph511} = 601$ photons), as explained in the Section II-B.

Fig. 7 and Fig. 8 show the simulated and measured spectra of the whole DoPET system acquisition of LYSO intrinsic radioactivity taken in single and coincidence modes, respectively. Since the density of ^{176}Lu inside the crystal can be calculated using the density of natural Lu present in the LYSO crystal, the intensities are presented as absolute values and are given in counts/s.

Fig. 7 shows the measured and simulated spectra of LYSO intrinsic radioactivity acquired in single mode. The simulated spectrum that uses the optical model (Fig. 7(b)) presents a much better agreement with the measured spectrum. The 88 keV peak is suppressed in the measured spectrum due to threshold settings applied in the associated electronics to avoid electronic noise. The other differences between both simulated spectra show that the degradation of the energy resolution in the measured spectrum is due to the optical photon attenuation along the crystal together with DoPET linear energy calibration. This effect is noticeable at the 202 and 307 keV peaks and in the long tail formed in the high energy part of the spectrum. DoPET uses the 511 keV peak as energy reference for linear calibration and this peak is associated with an energy deposition at the front of the crystal. This means that DoPET will register a higher energy value when an energy deposition occurs near the PMT, because the optical photons collected by the PMT will not be attenuated as much as an energy deposition further away the PMT. Thus, the same deposited energy will be registered as different values, and, for DoPET case, the difference between these values is not negligible.

TABLE V
COUNT RATES OBTAINED WITH SIMULATED AND MEASURED RESULTS OF THE LYSO CRYSTAL INTRINSIC RADIOACTIVITY

	count rates (cps)	
	singles	coincidences
experimental	16883	65.1
simulated	16820	63.2

Fig. 8 exhibits the measured and simulated spectra of LYSO intrinsic radioactivity acquired in coincidence mode. The coincidence events occur due to the detection of the emitted electron in one of the heads and the detection of at least one the subsequent gamma photons in the other head. With the exception of the suppressed peak of 88 keV, all the other peaks are present. Concerning the intensity of the peaks, the 307 keV peak of the simulated spectrum without optical model (Fig. 8(a)) is higher than the measured one. The agreement is much better with the inclusion of the optical model (Fig. 8(b)).

The count rates obtained for the full spectra are also in a good agreement, as can be seen in Table V. The count rates values represent only the background noise. Dead time and pile up losses are negligible in this situation of data acquisition at low count rates.

The measured and simulated spectra of a ^{22}Na point-like source at the center of the field of view and acquired in single mode are shown in Fig. 9. In this situation, the activity value of the ^{22}Na source used in the experiment is not precise, presenting a uncertainty of 30%. Therefore, the spectra is normalized by the area and the intensity, given in counts/s, is arbitrary. The LYSO

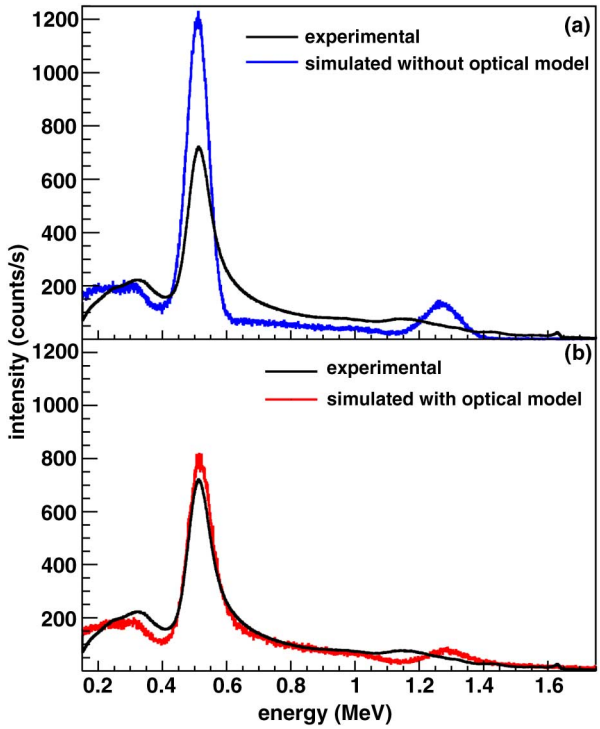

Fig. 9. Comparison of the simulated DoPET spectra without (a) and with (b) the use of the optical model, with the measured spectrum of a $^{22}\mathrm{Na}$ point-like source located in the center of the field of view acquired in single mode. The LYSO crystal intrinsic radioactivity ($^{176}\mathrm{Lu}$) is also considered in the spectra.

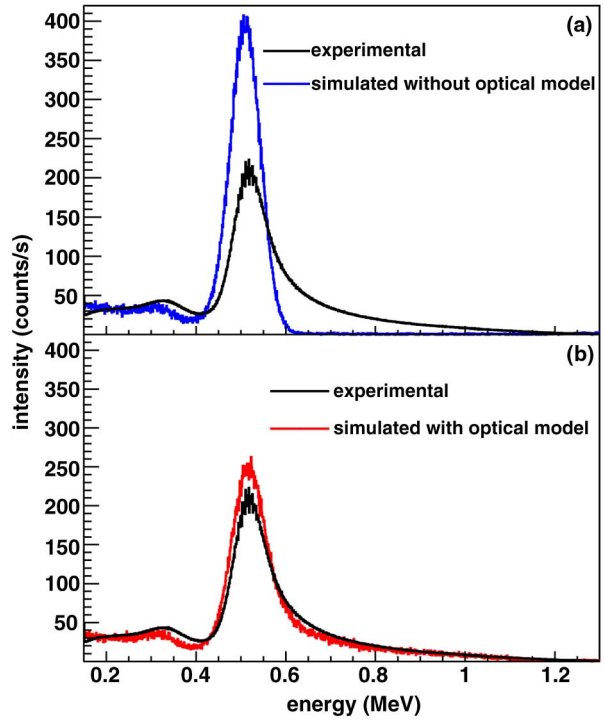

Fig. 10. Comparison of the simulated DoPET spectra without (a) and with (b) the use of the optical model, with the measured spectrum of a $^{22}\mathrm{Na}$ point-like source located in the center of the field of view acquired in coincidence mode. The LYSO crystal intrinsic radioactivity ($^{176}\mathrm{Lu}$) is also considered in the spectra.

crystal intrinsic radioactivity ($^{176}\mathrm{Lu}$) is also considered in the spectra.

A good agreement was obtained using the optical model (Fig. 9(b)) to describe the long tail beginning at 511 keV. However, the 1275 keV peak from the $^{22}\mathrm{Na}$ source appears in a shifted position that it is not very well described in the present simulation results. The scattering part of the spectra between the energies 150–400 keV are also presented in a slightly different position. These differences can be associated with the LYSO non-proportionality of the light yield [24] or even with an electronic gain calibration, which were not considered in this simulation.

Fig. 10 exhibits the measured and simulated spectra, acquired in coincidence mode, of a $^{22}\mathrm{Na}$ point-like source located in the center of the field of view (FOV) of DoPET. The LYSO crystal intrinsic radioactivity ($^{176}\mathrm{Lu}$) is also considered in the spectra. The spectra were obtained with a low energy cut at 150 keV. Again, the simulated spectrum with the proposed optical model (Fig. 10(b)) has a much better agreement with the experimental spectrum. The long tail present at the end of the experimental spectrum is reproduced when taking into consideration optical interactions in the scintillator.

Due to this long tail, the upper energy threshold of DoPET was previously set to 850 keV, instead of the commonly used values (600 or 650 keV). From the data shown in Fig. 10, it was determined that, even when the upper energy threshold is set at 850 keV, around 10% of the coincidence events is not registered by DoPET.

The use of the proposed optical model was shown to require much less computation time when compared to a DoPET simulation with GATE optical processes enabled. As an example of the usefulness of the optical model with an AMD Sempron 1.6 GHz based CPU, a DoPET simulation of a point-like $^{22}\mathrm{Na}$ source in the center of the field of view using the optical model needed around 7 hours of computation time. Performing a short DoPET simulation with GATE optical processes enabled and extrapolating the obtained time processing to a simulation with the same number of events of the example, we estimated that a DoPET simulation using GATE optical processes would require aproximately 10000 hours of time processing, being about 1400 times slower.

IV. Discussion and Conclusion

A time efficient optical model was proposed for GATE simulation of a LYSO scintillation matrix coupled to a PMT to predict the energy spectra and to avoid an excessively long computation time when activating the optical processes in GATE. The use of the proposed optical model was shown to be around three orders of magnitude faster than a DoPET simulation with GATE optical processes enabled.

The dual planar head DoPET was simulated using GATE and this optical model to compare experimental and simulated energy spectra as well as to demonstrate the usefulness of the model.

Simulations without and with modeling of the optical photon attenuation along each LYSO crystal element were performed. A very good agreement was found between experimental and simulated data with the inclusion of the proposed optical model. The results indicate that optical interactions inside the crystal elements play an important role on the energy resolution and

induce a considerable degradation of the spectra information acquired by DoPET.

The calibration procedure adopted by DoPET is appropriate for its clinical applications, but it does not take into consideration the non-linear detector response noticed in Fig. 9.

Moreover, it was determined that, even when the upper energy threshold is set at 850 keV, around 10% of the coincidence events is not registered by DoPET. Thus, it is possible to improve the system detection efficiency by increasing the upper energy threshold.

Finally, the same approach employed by the proposed optical model could be useful to simulate a scintillation matrix coupled to a PMT, as commonly employed in PET/SPECT detectors, using single [8], [26] or dual readout scheme [27], [28].

REFERENCES

[1] H. Zaidi, "Relevance of accurate Monte Carlo modeling in nuclear medical imaging," *Med. Phys.*, vol. 26, pp. 574–608, Apr. 1999.

[2] S. Jan *et al.*, "GATE: A simulation toolkit for PET and SPECT," *Phys. Med. Biol.*, vol. 49, pp. 4543–4561, 2004.

[3] S. Agostinelli *et al.*, "Geant4—A simulation toolkit," *Nucl. Instrum. Methods Phys. Res. A*, vol. A506, pp. 250–303, Jul. 2003.

[4] Y. Chen, B. Liu, J. M. O'Connor, C. S. Didier, and S. J. Glick, "Characterization of scatter in cone-beam CT breast imaging: Comparison of experimental measurements and Monte Carlo simulation," *Med. Phys.*, vol. 36, pp. 857–869, 2009.

[5] C. O. Thiam, V. Breton, D. Donnarieix, B. Habib, and L. Maigne, "Validation of a dose deposited by low energy photons using GATE/GEANT4," *Phys. Med. Biol.*, vol. 53, pp. 3039–3055, 2008.

[6] G. Santin, S. Staelens, R. Taschereau, P. Descourt, C. R. Schmidtlein, L. Simon, D. Visvikis, S. Jan, and I. Buvat, "Evolution of the GATE project: New results and developments," *Nucl. Phys. B*, vol. 172, pp. 101–103, 2007.

[7] *GATE User's Guide V4,* GATE Collaboration, Jun. 2009.

[8] R. R. Raylman, S. Majewski, B. Kross, V. Popov, J. Proffitt, M. F. Smith, A. G. Weisenberger, and R. Wojcik, "Development of a dedicated positron emission tomography system for the detection and biopsy of breast cancer," *Nucl. Instrum. Methods Phys. Res. A*, vol. A569, pp. 291–295, Dec. 2006.

[9] H. Alva-Sánchez, A. Martínez-Dávalos, E. Moreno-Barbosa, B. Hernández-Reyes, T. Murrieta, C. Ruiz-Trejo, M. Brandan, and M. Rodríguez-Villafuerte, "Energy calibration of individual crystals in a LYSO pixelated array for microPET detection modules using Voronoi diagrams," *Nucl. Instrum. Methods Phys. Res. A*, vol. A596, pp. 384–389, Nov. 2008.

[10] Y. Tai, A. Ruangma, D. Rowland, S. Siegel, D. F. Newport, P. L. Chow, and R. Laforest, "Performance evaluation of the microPET focus: A third-generation microPET scanner dedicated to animal imaging," *J. Nucl. Med.*, vol. 46, pp. 455–463, Mar. 2005.

[11] S. Vecchio, F. Attanasi, N. Belcari, M. Camarda, G. Cirrone, G. Cuttone, F. Di Rosa, N. Lanconelli, S. Moehrs, V. Rosso, G. Russo, and A. Del Guerra, "A PET prototype for "In-Beam" monitoring of proton therapy," *IEEE Trans. Nucl. Sci.*, vol. 56, no. 1, pp. 51–56, Feb. 2009.

[12] J. S. Huber, W. W. Moses, W. F. Jones, and C. C. Watson, "Effect of 176Lu background on singles transmission for LSO-based PET cameras," *Phys. Med. Biol.*, vol. 47, pp. 3535–3541, Oct. 2002.

[13] P. Rodrigues, A. Trindade, and J. Varela, "Clear-PEM system counting rates: A Monte Carlo study," *J. Instrum.*, vol. 2, p. P01004, 2007.

[14] N. Belcari, A. Del Guerra, M. Camarda, L. Spontoni, S. Vecchio, and D. Bianchi, "Performance of a four-output front-end electronics for multianode PMTS readout of scintillator arrays," *Nucl. Instrum. Methods Phys. Res. A*, vol. A572, pp. 335–337, Mar. 2007.

[15] G. F. Knoll*, Radiation Detection and Measurement. 3rd*. New York: Wiley, 2000, pp. 247–248.

[16] I. Vilardi *et al.*, "Optimization of the effective light attenuation length of YAP:Ce and LYSO:Ce crystals for a novel geometrical PET concept," *Nucl. Instrum. Methods Phys. Res. A*, vol. A564, pp. 506–514, Aug. 2006.

[17] R. Mao, L. Zhang, and R.-Y. Zhu, "Optical and scintillation properties of inorganic scintillators in high energy physics," *IEEE Trans. Nucl. Sci.*, vol. 55, no. 4, pp. 2425–2431, Aug. 2008.

[18] *Geant4 User's Guide for Application Developers,* Geant4 Collaboration, Jun. 2009.

[19] A. Levin and C. Moisan, "A more physical approach to model the surface treatment of scintillation counters and its implementation into DETECT," in *Proc. IEEE Nuclear Science Symp. Conf. Rec.*, 1996, vol. 2, pp. 702–706.

[20] C. Moisan, A. Levin, and H. Laman, "Testing scintillation transport models with photoelectron yields measured under different surface finishes," in *Proc. IEEE Nuclear Science Symp. Conf. Rec.*, 1997, vol. 1, pp. 824–828.

[21] D. Motta and S. Schönert, "Optical properties of bialkali photocathodes," *Nucl. Instrum. Methods Phys. Res. A*, vol. A539, pp. 217–235, Feb. 2005.

[22] Hamamatsu Technical Information, H8500 PSPMT Series 2009.

[23] J. Allison *et al.*, "Geant4 developments and applications," *IEEE Trans. Nucl. Sci.*, vol. 53, no. 1, pp. 270–278, Feb. 2006.

[24] A. Nassalski, M. Kapusta, T. Batsch, D. Wolski, D. Mockel, W. Enghardt, and M. Moszynski, "Comparative study of scintillators for PET/CT detectors," *IEEE Trans. Nucl. Sci.*, vol. 54, no. 1, pp. 3–10, Feb. 2007.

[25] A. Del Guerra, A. Bartoli, N. Belcari, D. Herbert, A. Motta, A. Vaiano, G. Di Domenico, N. Sabba, E. Moretti, G. Zavattini, M. Lazzarotti, L. Sensi, M. Larobina, and L. Uccelli, "Performance evaluation of the fully engineered YAP-(S)PET scanner for small animal imaging," *IEEE Trans. Nucl. Sci.*, vol. 53, no. 3, pp. 1078–1083, Jun. 2006.

[26] S. Surti, J. Karp, A. Perkins, R. Freifelder, and G. Muehllehner, "Design evaluation of A-PET: A high sensitivity animal PET camera," *IEEE Trans. Nucl. Sci.*, vol. 50, no. 5, pp. 1357–1363, Oct. 2003.

[27] M. Abreu, J. Aguiar, F. Almeida, P. Bento, B. Carrico, M. Ferreira, F. Goncalves, C. Leong, F. Lopes, P. Lousa, M. Martins, N. Matela, P. Mendes, R. Moura, J. Nobre, N. Oliveira, C. Ortigao, L. Peralta, R. Pereira, J. Rego, R. Ribeiro, P. Rodrigues, J. Sampaio, A. Santos, L. Silva, P. Sousa, I. Teixeira, A. Trindade, and J. Varela, "Design and evaluation of the clear-PEM scanner for positron emission mammography," *IEEE Trans. Nucl. Sci.*, vol. 53, no. 1, pp. 71–77, Feb. 2006.

[28] J. Huber, W. Choong, J. Wang, J. Maltz, J. Qi, E. Mandelli, and W. Moses, "Development of the LBNL positron emission mammography camera," *IEEE Trans. Nucl. Sci.*, vol. 50, no. 5, pp. 1650–1653, Oct. 2003.